Development and initial application of a blade design methodology for overspeed power-regulated tidal turbines

Katie Gracie-Orr*, Thomas M. Nevalainen, Cameron M. Johnstone

Energy Systems Research Unit, Dept. of Mechanical and Aerospace Engineering, University of Strathclyde, Glasgow,Scotland, G1 1XJ

Robynne E. Murray, Darrel A. Doman, Michael J. Pegg

Dept. of Mechanical Engineering, Dalhousie University, PO Box 15000, Halifax, Nova Scotia, Canada, B3H 4R2

Abstract

The range and variability of flow velocities in which horizontal axis tidal stream turbines operate introduces the requirement for a power regulation method in the system. overspeed power regulation (OSPR) has the potential to improve the structural robustness and decrease the complexity associated with active pitch power regulation methods, while removing the difficulties of operating in stalled flow. This paper presents the development of a methodology for the design of blades to be used in such systems. The method requires a site depth, maximum flow velocity and rated power or flow speed as input parameters. The pitch setting, twist and chord distribution were set as input parameters, variable through the use of alteration functions. Rotor performance has been broken down into OSPR performance metrics which consider coefficients of power and thrust, and cavitation inception. Three visual-numerical tools have been developed: the OSPR performance metrics were used in conjunction with a one-at-a-time sensitivity analysis approach to develop a design space; cavitation inception analyses gave plots of converging cavitation and pressure terms for each blade section; the local angle of attack and torque distribution across the blade designs were plotted at key turbine operation states. Alterations to pitch setting and twist distribution are shown to have most impact upon this design requirement; coupled with such alterations, targeted changes to the chord distribution have been shown to increase the maximum efficiency. The prevention of cavitation has been highlighted as a driver for speed-limiting design alterations. While facilitating blade design, the methodology also produces experiential knowledge which can be stored, and shared in graphical format.

Keywords: Tidal turbine, blade design, overspeed, power regulation, design methodology, sensitivity analysis, blade element momentum theory

1. Introduction

Cost reduction, in order to become economically competitive with other sources of renewable energy, is essential for the development of the tidal energy industry. It is therefore desirable to remove as many of the vulnerabilities, complexities and systems which add cost to tidal turbine technologies. One aspect of tidal turbine systems in which this may be achievable is the power regulation system. This paper outlines a methodology developed for the design of blades for horizontal axis tidal stream turbines (HATSTs) in which OSPR will be the means of power control, with the goal of cost reduction over alternative power regulation methods.

*Corresponding author
Email address: katiegracieorr@gmail.com (Katie Gracie-Orr*)

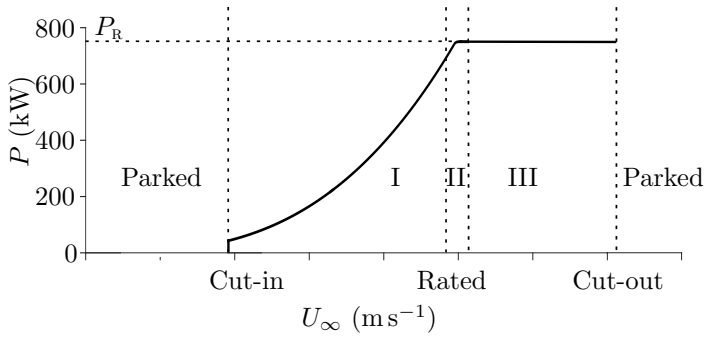

Figure 1: Operational regions for HATSTs in terms of inflow velocity and power.

1.1. Power Regulation

The periodic variability of tidal flow velocities gives rise to an according periodic variability in the power available in the flow. HATST systems achieve rated power, P_R, when the tidal flow reaches the rated flow speed, $U_{\infty R}$. For the greater part of the tidal cycle, flow velocities are less than or equal to $U_{\infty R}$, and turbines are generally operated in such a way as to maintain the rotor efficiency, C_P at the optimum value, C_{PO}. C_P is a function of the ratio between the speed of the tip speed ratio, λ, defined as:

$$\lambda = \frac{\Omega R}{U_\infty} \, . \tag{1}$$

C_P is maintained at the optimum value through means of maximum power point tracking (MPPT), in which operation mode the turbine control keeps λ at the optimum value, λ_O. The variability of tidal flow velocity means that higher values of power than P_R are frequently available, but for only a small percentage of the time. It is therefore more economically efficient to optimise the turbine system to capture P_R at a value less than the maximum flow velocity, $U_{\infty max}$, and to spill or *regulate* the excess power when the available power exceeds the rated value. In this manner, the turbine system is operated at its most efficient for a greater proportion of time and the generator, drive train components and rotor can be protected from electrical and structural over-loading.

This is summarised in Fig. 1. In region I the flow velocity increases from the cut-in speed, $U_{\infty cut\text{-}in}$, to the rated speed, $U_{\infty R}$, the turbine is operated in MPPT and the power captured increases with the cube of the velocity. In region II, at a flow velocity slightly lower than $U_{\infty R}$, the power captured nears P_R and the system transitions from operation in MPPT to power regulation operation. In region III, ideally, P_R will be maintained throughout, up to a cut-out speed. To achieve this, C_P must be reduced in line with the increase in U_∞.

MPPT and power regulation can be achieved with four main configurations: fixed speed (FS) operation of a turbine with fixed pitch (FP) blades, FS operation of a turbine with variable pitch (VP) blades, variable speed (VS) operation of a turbine with FP blades, and VS operation of a turbine with VP blades. The latter two are the most common for HATST designs to date, and can each be combined with either permanent magnet synchronous generators (PMSGs) or doubly-fed induction generators (DFIGs), decoupled from the grid through appropriate power electronics to allow VS operation and power conditioning.

In VS VP turbines, active alterations are made to the blade pitch setting angle, β, (see Fig. 2) during operation, allowing either *pitch to stall* or *pitch to feather* power control methods [1]. In VS FP turbines, the electromagnetic torque, Q_{em}, in the generator which counters the mechanical torque produced at the rotor, Q_{mech}, is controlled to vary the rotational velocity, Ω, of the shaft and rotor. Normally, this control over Ω is used to put the blades into stall, lending the term *speed-assisted stall control*. As Fig. 2 indicates, alterations to β and Ω result in changes in the relative velocity, W_r, and the angle at which this encounters the blade section - the local angle of attack - α_r. Accounting for the effect of the rotor's presence in the flow with axial

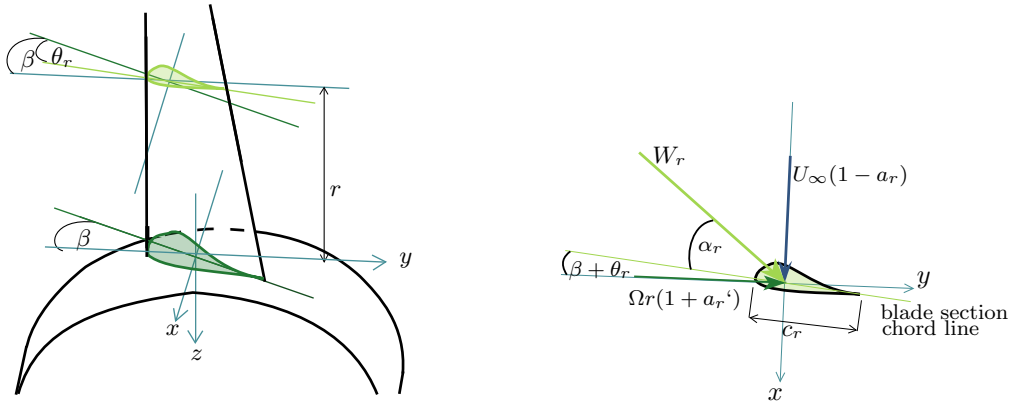

Figure 2: *Left*: Orthogonal view diagram of rotor, blade at top dead centre position, coordinate system and angle definitions. β is measured from rotor plane and has a positive value here; θ_r is measured from the blade root chord line and is negative here. *Right*: Plan view diagram of 2D flow vectors for a blade section, also showing definition of chord.

and tangential induction factors, a and a', the vector relationship is given by

$$W_r = \sqrt{((1-a_r)U_\infty)^2 + ((1+a_r')\Omega r)^2} \tag{2}$$

Fig. 2 and Eq. (2) illustrate that power regulation methods can manipulate β and Ω, to control W_r and α. The power and thrust developed at the rotor depend on the lift and drag forces developed by each blade section; these vary with W_r and α_r. Thus, control of W_r and α_r allows control of mechanical power and thrust.

The pitching capability of VP systems is generally achieved via an electronic controller with a hydraulic system, and sometimes with an electronic motor system [2]. VP blades allow rapid, blade-specific and, often, very sensitive adaptations to the flow conditions and thus facilitate increased energy capture, smoother power flow and reduced structural loading compared to FP blade systems. VP blades can also develop high starting torques which can increase the annual energy capture, and can bring the rotor to a slower speed before application of the parking break [3]. However, pitching the blades into stall introduces challenges such as stall delay, reduced damping in separated flow, and hysteresis of reattachment. On the other hand, while pitching to feather maintains fully attached flow, comparably large pitch excursions are required, introducing a time-lag. This can have consequences on power and structural loads. Active pitch mechanisms add mechanical and structural complexity to the system, decreasing the robustness and increasing the turbine's vulnerability [1]. VP blade connections to the hub must include bearings which are required to withstand the entire blade root bending moments and forces resulting from the blade's interaction with the flow, while maintaining the pitching ability of the connection [4].

In FP blade systems, on the other hand, the bolt or stud-type connections between the blade root and hub are required simply to hold the blades in place, giving a more structurally robust system. However, FP blades cannot adapt to individually-experienced flow conditions and, even in VS operation, rotors with FP blades generally have a reduced energy capture and increased structural and fatigue loading characteristic than a rotor with VP blades [2] - the challenges associated with separated flow also apply to speed-assisted stall regulation. A further disadvantage is the overcapacity required within the generator to produce the electromechanical torque that regulates rotor speed [5]. This unavoidable aspect of VS stall regulated machines adds capital and mass to the turbine, increasing its cost. Because the blades are fixed in position, high loads can be experienced in parked mode past the cut-out velocity, requiring either a stronger mooring system or a nacelle-yaw capability.

In [6], Whitby and Ugalde-Loo compared the performance of a VS VP (pitch to feather) and a VS FP

turbine and control system, modelled in GH Tidal Bladed. They found that the VS VP pitch to feather system was more stable in power regulation and had lower loads across the entire operation, particularly in deep stall. The VS VP also had a higher energy capture. This is due to the reduction in flow states for which a FP rotor can maximise efficiency compared to a VP alternative.

Though there are disadvantages to consider, the robustness of FP blades is a significant advantage, particularly for the tidal industry in which access limitation can augment down-time. In the wind industry, as reported in an evaluation of an extensive 10 year study of 350 MW worth of wind turbines [7], failures in the pitching mechanisms - considering pitch drives, bolted joints and bearings but not the blades themselves - were the driving factor for the 85% higher rotor failure rate of pitch regulated turbines than passive stall regulated ones.

1.2. The Overspeed Method

The advantages of avoiding stall and having FP blades can be combined by regulating power with VS FP turbine which goes into overspeed, rather than stall, when $U_{\infty \mathrm{R}}$ is exceeded. In such an OSPR turbine system, Q_{em} is reduced during power regulation, allowing Ω to increase, effecting an increase in the magnitude of W, and a decrease in α. This technique, too, can be used to reduce C_{P} in a predictable way. Detailed discussion and design of the electromagnetic control aspects of turbines operated with speed control are out-with the scope of this paper. However, there is much literature on the topic of speed control, including the control schemes discussed in [6] and [8]. It would seem that a PMSG regulated by pulse-width-modulation would be a reasonable solution. Within such a control scheme the required Q_{em} could be found from a look-up table according to the measured Q_{mech} and Ω at each flow state. In [9], Winter suggests that Ω can be read from an encoder and discusses the stability of such a control scheme.

As reported in [10], practical experiments with Q_{em} control in a wind tunnel showed that the method is physically possible, and highlighted some engineering challenges which need to be overcome if OSPR is to become practicable for tidal turbines. The operation of turbine rotors at high values of Ω results in high values of terminal voltage, and cavitation also becomes an issue of concern. Some turbine blades have C_{T} characteristics in the higher λ region which would lead to very high thrust forces - this would also need to be addressed. Furthermore, centrifugal forces, which are proportional to the square of the Ω, become greater. With higher Ω values, such as in wind turbine operation, these forces can provide "centrifugal relief" to the axial thrust force experienced by the blades [3] but, if causing large enough tensile stress in the radial direction, could also be a cause of, or contribution to, blade failure.

High voltages in a turbine require thicker electrical insulation, which adds size and mass, increasing deployment costs. High structural loads require stronger, more expensive station-keeping designs; likewise, high blade loads require more or stronger materials. As discussed in [11], cavitation on a blade degrades performance and can also cause extensive structural damage to the point of component destruction. Designing super-cavitating blades for turbines could, in theory, be an option; however, materials which can cope with the energy release from imploding cavities are costly. None of these options contribute to cost reduction. Addressing these engineering challenges with cost-effective solutions is essential before OSPR can be successfully used in a turbine system.

Research in the field of blade designs and design methodologies for overspeed control has been undertaken and presented in such papers as [9, 12, 13, 14, 15] which discuss and work to mitigate some of the issues discussed. A primary focus for blade development in these projects has been controlling the thrust forces as the tidal velocity increases. Though there has been discussion of the requirement for reduced maximum values of Ω [14], cavitation inception has not been discussed.

1.3. Aim of the design methodology

As concluded in [10], and demonstrated in [16], it would appear that these challenges may be overcome with a more rapid drop in efficiency as Ω increases, avoiding rotational velocities of such values as to introduce cavitation and voltage problems.

The blades of a tidal turbine are major contributors to turbine performance. By altering the design of the blades it is possible to significantly alter the relationships between C_{P}, C_{T} and λ. The aim of the present

research is to look into how the highlighted engineering challenges can be satisfactorily overcome with the use of a blade design methodology specifically developed for this purpose. The goals of this methodology are to facilitate the design of blades which maintain high values of optimum C_P, while resolving the discussed challenges by reducing the maximum rotor velocity. To achieve this, the methodology considers the criteria of importance in blade design noted in [17] - hydrodynamic, geometrical, structural and deployment site parameters - and also takes into account the proposed operating methodology. The inclusion of the control method in the blade design methodology has been explicitly considered in work undertaken by National Renewable Energy Laboratory (NREL), reported in [18].

In general, it is possible to consider any blade design alteration, and/or to couple these with any other design alterations. There are two extremes of possible blade design methodologies - incremental and algorithmic. This methodology was developed with the aim to: remove much of the time and expertise required in the incremental-alterations option; break down and open-up for viewing the "black-box" of the optimisation algorithm option; and produce information which provides some of the experiential knowledge gained by - and often limited to - the engineer and computer, respectively, in the alternative options. Alterations made by eye, randomly or incrementally would be exceedingly time-consuming, and a successful blade design may be long in the coming, unless the engineer has expertise or experience. On the other hand, it is possible to write optimisation algorithms which consider a wide range of blade shapes and optimise based on a set of objectives and constraints. An advantage of this option is that, once the algorithm and implementation programme have been developed, the time required to produce a blade design can be significantly reduced.

In the former case, the engineer uses experience to by-pass many of the options an algorithm would trial, based on an understanding of constraints and the relationships between inputs and outputs; however by the same necessary process of selection, the engineer may not consider possible options which could inform or improve the blade design. Furthermore, while either of these options can result in successful blades, it may not be standard for either process to output information on the impact of alterations to the blade design parameters. This, importantly, is experiential knowledge which would be useful in general for engineers working on turbines, and in particular for the development or fine-tuning of both the blade in design, and those of future turbine installations.

The methodology herein described, then, will have some of the advantages of each of the two extreme alternative approaches, and some of the disadvantages. It can be seen, therefore, as a balance between the two, with the further advantage of outputting useful information which can be stored and shared. The methodology has been specifically developed for the design of blades for use in OSPR tidal turbines, yet with alternative metrics could be easily applied in the design of FP blades for use with a different power regulation method. This paper describes the development of this methodology.

2. Methodology

2.1. Outline of the design methodology

The basis of the design methodology is to:

- define design requirements and boundary conditions based on site characteristics and turbine configuration
- establish base case performance with an existing blade design, using a verified numerical design tool
- modify the design of the blades in a series of alterations to the geometrical parameters, applied with function-based alterations
- simulate the performance of each new rotor design
- assess the impact made upon the suitability of the rotor for use in OSPR using visual-numerical tools, building up a picture of the influence of each geometrical parameter
- use the information and insight gained to meet the design requirements.

At this point in the development, the methodology is focused primarily on the hydrodynamic aspects of rotor design, and analysis of the structural properties of blade designs is limited to consideration of the C_T-λ curve. Tidal sites, at this stage, are considered to have a range of inflow velocities, from cut-in to cut-out, and it is assumed that the turbine will be parked and/or yawed above these flow speeds; the effect of turbulence and the velocity and depth-altering effects of waves are not yet incorporated into the methodology. No control system is implemented at this blade design stage, and therefore perfect transition from region I to III (Fig. 1) is assumed.

2.2. Performance Prediction Tools

As reported in [19], a Blade Element Momentum Theory (BEMT) tool has been developed and verified against several sets of empirical data, including data obtained in tow tank tests previously undertaken within this project; the greater detail of these tests was presented in [20]. This tool is considered to be valid for use in the design of tidal turbine blades and was used as such in this research.

Accurate BEMT predictions require appropriate aerofoil data - coefficients of lift, C_l, and drag, C_d, as they vary with the angle of attack, α_r, of the fluid onto the aerofoil - as an input. Aerofoil performance is highly sensitive to the Reynolds number, Re, free-stream turbulence and the Mach number. The velocities involved mean that the latter is not an issue for tidal turbines. In the case of an aerofoil, the definition for Re is given as

$$Re = \frac{\rho W c}{\mu} \ , \tag{3}$$

where ρ and μ are the density and dynamic viscosity of the working fluid, and c is the chord length. As will be discussed, the Re appropriate for the full scale rotor analyses undertaken in this work were in the range of 1x10^7. In the absence of physical test data at these Re, the design code XFOIL, developed to give computationally efficient and reasonable predictions of aerofoil performance, was used to obtain NREL S814 data at the appropriate Re. As reported by Drela in [21], XFOIL uses several empirically-based corrections to predict aerofoil performance which, as the developers note in [21], are reasonable data until just after stall. As discussed in [19], the BEMT code used in this project includes a Viterna-Corrigan correction for more accurate modelling of post-stall behaviour. Previous examples of the use of XFOIL for the prediction of aerofoil data for tidal turbine applications exist extensively in, for example, the projects reported in [22, 23, 24, 25]. The choice of the critical N_{crit} value for the e^N method, used by XFOIL to predict transition, was based on the recognition that tidal turbine rotors operate in a highly turbulent environment. As discussed in [26], to represent this large free-stream disturbance in XFOIL, lower values of N can be set. According to the XFOIL User Primer [27], setting N_{crit} to a value of 1 or less tells the programme to bypass transition. The sensitivity of the C_l and C_d predictions to N_{crit} in the range between $N_{crit} = 1$ and $N_{crit} = 2$ was found to be very low; an N_{crit} value of 2 was therefore selected as a best-fit value, setting transition to occur quickly due to large values of free-stream disturbances.

The BEMT code can be set to predict performance at any integer number of λ values spanning the C_P-λ curve from the extreme LHS to the runaway point. Densely populated curves allowed accurate interpolation of intermediate points with a linear method.

2.3. Design Operation and Requirements

The relationship between the flow vectors and the C_P and coefficient of thrust, C_T for a rotor design is commonly presented with performance curves such as those in Fig. 3. These characteristic curves describe rotor performance over the range of flow conditions between the fully-stalled condition on the far LHS, where $\lambda \to 0$, to the fully feathered condition, also termed the runaway point, on the far RHS, where $\lambda = \lambda_{rw}$.

2.3.1. Operation in Overspeed

Previous work [10] discussed the operation methodology for OSPR in terms of the flow regime and the required drop in C_P (to cap power at the rated value) and thus the required Ω, as U_∞ increases from $U_{\infty R}$ to $U_{\infty max}$.

The extent to which C_{P} must be reduced is also dependant on the rated wattage of the turbine. The following definitions are based on the commonly used terms for λ, C_{P} and C_{T}, defined in, for example, [11] and [3]. The definition of the maximum efficiency, C_{Po}, is

$$C_{\mathrm{Po}} = \frac{P_{\mathrm{R}}}{\frac{1}{2}\rho\pi R^2 U_{\infty\mathrm{R}}^3} \tag{4}$$

and the efficiency required at $U_{\infty\mathrm{max}}$, when the power regulation system is at its maximum operation point, C_{Povs}, is defined as

$$C_{\mathrm{Povs}} = \frac{P_{\mathrm{R}}}{\frac{1}{2}\rho\pi R^2 U_{\infty\mathrm{max}}^3} \tag{5}$$

This operation point is herein termed the overspeed point. The Ω at each of these operation points can be defined in a rearrangement of Eq. (1):

$$\Omega_{\mathrm{o}} = \frac{\lambda_{\mathrm{o}} R}{U_{\infty\mathrm{R}}} \tag{6}$$

and

$$\Omega_{\mathrm{ovs}} = \frac{\lambda_{\mathrm{ovs}} R}{U_{\infty\mathrm{max}}} \tag{7}$$

A full description of the performance of a rotor operating in OSPR also requires quantification of the thrust performance at the two key operating points. These are defined as:

$$C_{\mathrm{To}} = \frac{T_{\mathrm{R}}}{\frac{1}{2}\rho\pi R^2 U_{\infty\mathrm{R}}^2} \tag{8}$$

and

$$C_{\mathrm{Tovs}} = \frac{T_{\mathrm{ovs}}}{\frac{1}{2}\rho\pi R^2 U_{\infty\mathrm{max}}^2} \tag{9}$$

The methodology requires the value of P_{R} (or alternatively $U_{\infty\mathrm{R}}$) as an input. T_{ovs} and λ_{ovs} are dependent on the blade shape and the input set design variable, $U_{\infty\mathrm{max}}$. The values of T_{R} and λ_{o} are blade design variables, outputs of the methodology.

The operation range was defined as the range of flow conditions within which optimum point tacking - normal turbine operation - and power-regulation operation would exist. The local flow conditions across the entire operation range were then determinable from Eq. (1), noting that in the range $0 \leq U_{\infty} \leq U_{\infty\mathrm{R}}$, the operation would be held at the optimum point, λ_{o}, and in the range $U_{\infty\mathrm{R}} \leq U_{\infty} \leq U_{\infty\mathrm{max}}$, the operation would move from the optimum to the overspeed point, λ_{o} to λ_{ovs}.

2.4. Blade design parameters

2.4.1. Base Case Blade

It was necessary to define a base case blade design from which to make geometrical alterations, and from the performance of which to measure improvements. An existing blade design of NREL S814 aerofoil section was chosen; the NREL S814 was designed to have a high maximum lift, has the structural advantage of being relatively thick, and its insensitivity to surface roughness lends it to use in the biologically diverse and potentially sediment-carrying marine environment [28]. The base case blade geometry is detailed in Table 1, in which the blade length and chord geometries are expressed as a fraction of the total blade length, L_b, giving a non-dimensionalised, scalable blade design, independent of hub size. Illustrations of the base case blade design are included in Fig. 4a) and b); Fig. 4 c) and d) include the base case twist and chord distribution.

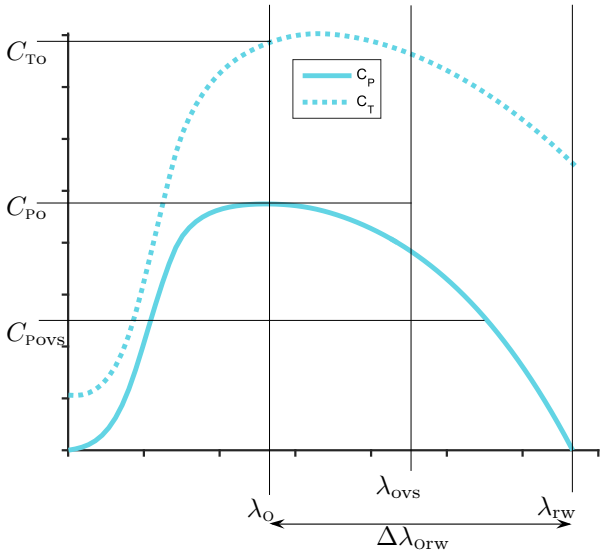

Figure 3: BEMT prediction of performance curves of base case, full-scale rotor, showing position of significant operating points and metrics of performance for overspeed power regulation

Table 1: Geometry of base case blade design

$r/L_b(-)$	$c_r/L_b(-)$	$\theta_r(^\circ)$
0	0.22	0
0.1	0.21	-4.9
0.2	0.21	-10.6
0.3	0.19	-14.2
0.4	0.18	-16.7
0.5	0.17	-18.3
0.6	0.16	-19.2
0.7	0.14	-19.9
0.8	0.13	-20.4
0.9	0.12	-20.8
1	0.09	-21.1
	β°	26.9

Table 2: The blade design parameters, manner and range of alterations made in the Stage One design changes

Parameter	**Alteration**	
	Manner	Range
β	Setting angle altered	$-7^\circ \leq \delta\beta \leq 13^\circ$
θ_r	Proportionally linear alterations applied from zero at root to ζ at tip	$-17^\circ \leq \zeta \leq 17^\circ$
c_r	Multiplied by scaling factor τ	$0.1 \leq \tau \leq 3$
	Stage Two Alterations	
c_r	Proportionally linear addition to chord length, from zero at root to $\mathrm{T} \cdot c_{\mathrm{tip}}$ at tip	$0.3 \leq \mathrm{T} \leq 1.3$
c_r	Parabolic addition to chord length, from zero at root to $\psi \cdot c_{\mathrm{root}}$ at tip to zero at tip, with $\mathrm{T} = 0.5$	$0.2 \leq \psi \leq 1.8$
	Stage Three Alterations	
θ_r	Proportionally linear alterations applied from zero at root to ζ at tip	$-1^\circ \leq \zeta \leq 17^\circ$

2.4.2. Blade Design Parameter Alterations

The major aspects of blade design which were set as variable parameters in the development of this methodology were the blade pitch, β, the twist distribution, θ_r and the chord distribution, c_r. The definitions of these parameters are indicated in Fig. 2.

Each parameter was altered with functions as described in Table 2, giving series of blade designs, each with discrete alterations made, first over the range and in the manner described in the Stage One alterations section of Table 2. Following analysis of these blade designs, a second set of targeted function-based alterations were made to the chord distribution, as detailed in the Stage two alterations section of Table 2.

Fig. 4 illustrates the types of design changes made, giving an example of one blade iteration with a proportionally linear twist alteration and one with the chord scaled up.

2.5. Overspeed Power Regulation Performance Metrics

Fig. 3 shows the BEMT prediction of the C_{P} and C_{T} performance of the base case rotor. This was used to identify the characteristics of rotor performance which were advantageous for operation in OSPR, and those which were detrimental. Important features of this figure are:

- The optimum operating point where λ is such that the maximum efficiency, C_{Po}, occurs. At this operating point, λ is defined as λ_{o} and C_{T} as C_{To}.
- The runaway point, where efficiency drops to zero and C_{Prw}, C_{Trw} and λ_{rw} occur.
- And, between these two, some position where C_{Povs} and therefore C_{Tovs}, λ_{ovs} and Ω_{ovs} occur.

As Eq. (5) indicates, the value of C_{Povs}, and thus of λ_{ovs}, C_{Tovs} and Ω_{ovs}, depend on the site and turbine configuration.

As discussed, a steeply negative gradient on the RHS of the C_{P}-λ, to give the required drop in C_{P} with a reduced increase in λ, was the key design requirement. Improvements in this characteristic would result in rotor performance curves of an increasingly appropriate shape for OSPR, avoiding high rotational velocities. The metric used to measure this - and therefore the primary metric - was $\Delta\lambda_{\mathrm{o\,rw}}$. A second metric was the rotor's angular velocity at the overspeed point, Ω_{ovs}, directly quantifying Ω at the crucial operation

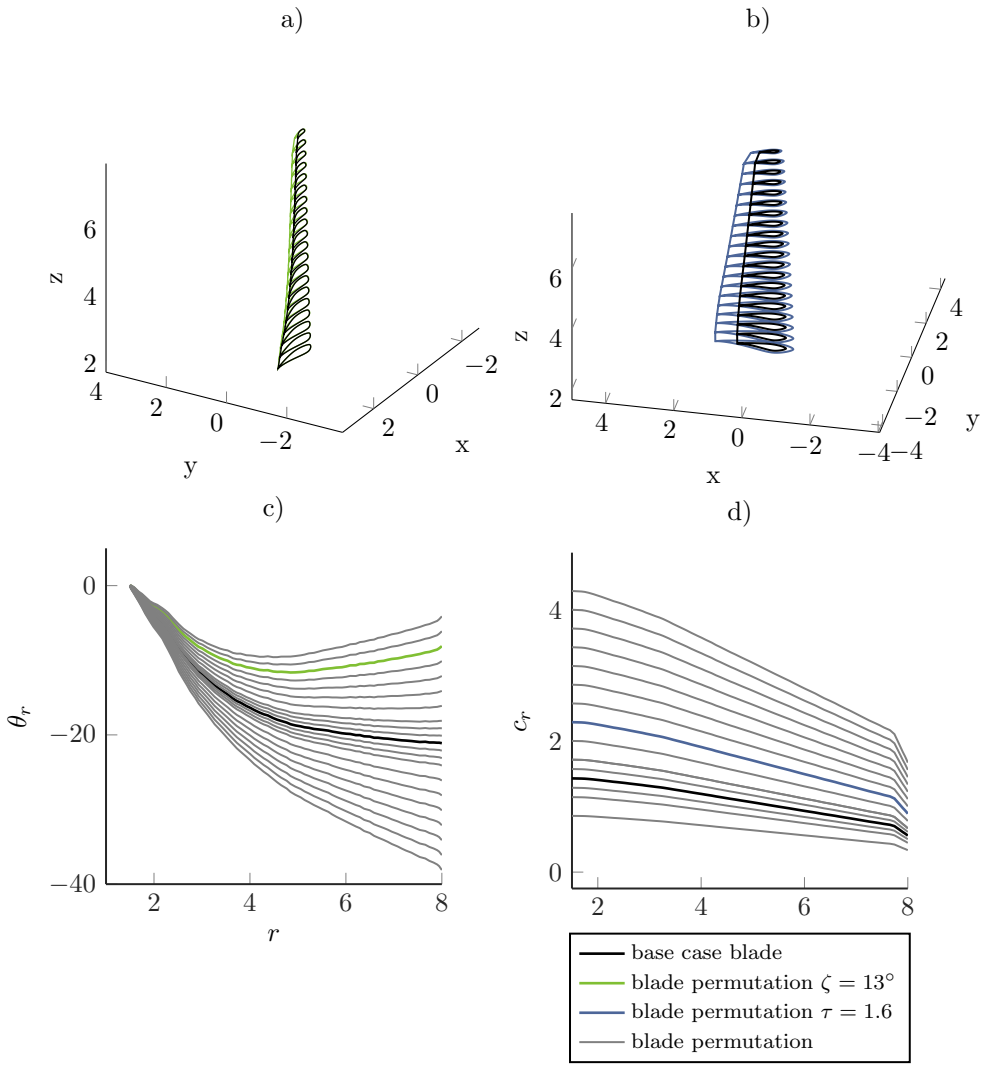

Figure 4: Graphical representation of comparison to base case blade of: a) and c) blade design iterations with proportionally linear twist alterations, including to $\zeta = 13°$ at the tip; b) and d) blade design iterations with scaled chord alterations, including by $\tau = 1.6$.

state. Both these metrics were required as the former gave insufficient information to ascertain whether cavitation would occur, but the latter gave no clear indication of the effect of a blade parameter change on the *shape* of the performance curve. As the value of C_{Po} is so influential on the annual energy output from a turbine, it was of benefit in this blade design process to gain an appreciation of blade design alterations which cause changes in the maximum efficiency the rotor could achieve. C_{Po} was therefore set as the third metric, improvements in which were measured as positive changes from the base case. C_{To} was set as the fourth metric, providing information on the effect of blade design changes on the thrust characteristics. This is a useful metric as C_{T} may be a limiting criterion; increases from the base case value in this metric were therefore defined as negative effects.

This reasoning gave a set of four performance metrics to be used in this design methodology:

- $\Delta\lambda_{\mathrm{o\ rw}}$
- Ω_{ovs}
- C_{Po}
- C_{To}.

A general formula was used to calculate change in each metric, M, between the base case blade design value, M_{bc}, and that of each discrete design iteration, M_j. This formula took the form

$$M = \frac{M_{\mathrm{bc}} - M_j}{M_{\mathrm{bc}}} \tag{10}$$

for all cases except for C_{Po}, for which it had the form

$$M = \frac{M_j - M_{\mathrm{bc}}}{M_{\mathrm{bc}}}\ . \tag{11}$$

These fractional values were then expressed as percentages. The impact of blade design alterations could then be measured as the percentage change in the defined metrics. Setting the equations so as to define a positive change as an improvement, and negative change as indicating detrimental effects facilitated the sensitivity analysis impact assessment described in Section 2.8.1.

2.6. Cavitation

2.6.1. Method of cavitation analysis

Cavitation, as discussed in [11], is likely to occur in a fluid in which minute nuclei - groups of molecules of gas or vapour - encounter a reduction in pressure of the surrounding fluid which allows their growth into fully-formed cavities. Though it is a simplification to state that this occurs when the local fluid pressure, p_{L}, on a blade reaches the vapour pressure of the fluid, p_{v}, comparison between these two values is seen to be a fair measure of the likelihood of cavitation inception, should the flow environment continue in this state. This method of cavitation inception analysis has been previously used in, for example, the projects reported in [23, 24, 29], in each of which verification by comparison to experiments presented in the former has shown the method to be appropriate. Furthermore, this was the approach taken in blade design projects presented in [30]. This was therefore the method adopted in the present research.

As in [11], the local pressure distribution across a 2D aerofoil can be expressed with the coefficient of local pressure, defined as

$$C_{\mathrm{pres}} = \frac{p_{\mathrm{L}} - p_{\mathrm{or}}}{\frac{1}{2}\rho W_r^2} \tag{12}$$

of which the minimum negative value - that is, the coefficient of the maximum suction pressure - is termed $C_{\mathrm{pres,\ min}}$. The value of $C_{\mathrm{pres,\ min}}$ on a 2D aerofoil changes with α, and can occur at the aerofoil nose, back or front faces.

A dimensionless cavitation number for a blade section at radius r can be defined, again as in [11], [31] and [24], as:

$$\sigma_r = \frac{p_{or} - p_v}{\frac{1}{2}\rho W_r^2} \tag{13}$$

where $\frac{1}{2}\rho W_r^2$ is the dynamic pressure, and the absolute hydrostatic pressure, p_{or}, is defined as

$$p_{or} = p_{atm} + \rho g h_r \tag{14}$$

The hydrostatic pressure will be at its smallest value when a blade is in the top dead-centre position, meaning that if cavitation occurs on a rotor, it will occur first on a blade at this position.

As Eqs. (12) and (13) show, if the minimum negative p_{Lr} on a blade section is equal to p_v, then σ_r will be equal to the minimum negative value of C_{presr}. Therefore, an inception cavitation number can be defined as

$$\sigma_{ir} = -C_{\text{pres min}r} \tag{15}$$

Assessment of cavitation inception on the blade designs therefore required comparison of σ_r and σ_{ir}, for each blade element, at each operation point. The $C_{\text{pres, min}}$ data required for this analysis was output from the aforementioned XFOIL analyses, as a function of α.

2.7. Full scale base case

2.7.1. Boundary Conditions

From the non-dimesionalised base case blade design, a full scale base case was required to be developed. Because this design methodology considers the turbine operation technique a meaningful cavitation analysis would require, as indicated by the foregoing discussion, information on:

- the site velocity profile
- the turbine hub depth
- the turbine rating
- blade length and hub radius, R_h

To define these boundary conditions, a full-scale turbine scenario was created in which a turbine with a radius, R, of 8 m was sited in a flow field of maximum flow speed of just over 6 knots, at a shaft depth of 20 m. A rated flow speed of 1.28 knots was set, allowing the optimum efficiency of the turbine to be determined from Eq. (4), and giving chord Re in the range of $1\text{x}10^7$. The value used for p_v was 1374.1Mpa, taken from [32] for seawater at 12°C. The remaining operating conditions were determined as previously discussed. The blade length was determined based on R and R_h. R_h was set as 2 m which may seem rather large, but initial developments of the methodology at the prototype scale indicated that large blade root chords would be required to meet the design requirements and there had to therefore be room on the hub for large blade root sections. The blade root pitch setting was optimised for C_p for these conditions, giving the best case scenario for the base case blade.

A further simplifying condition assumed for the development stage of this work was that the flow onto the turbine was at all times un-yawed and that free-stream disturbances would have no effect on the flow velocities or angles.

2.7.2. Aerofoil Data

Defining the flow regime and turbine configuration, as discussed in Section 2.2, allowed calculation of the appropriate Re from Eq. (3) so that relevant aerofoil data could be obtained. Fig. 5 shows the aerofoil data input to the BEMT tool. As the figure shows, the optimum α for this aerofoil at this Re is 7.5°; blade sections operating at this α will develop the greatest lift to drag force ratio.

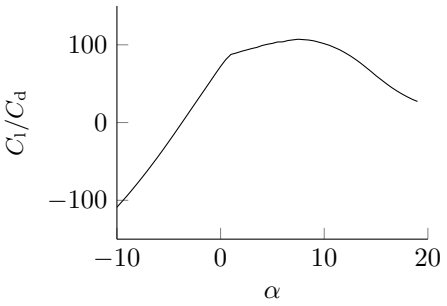

Figure 5: Plot of C_l/C_d with α at $Re = 1 \cdot 10^7$

2.8. Visual and Numerical Performance Analysis Tools

Several component tools were developed in the design of this methodology, which provide visual feedback based on numerical outputs from the analysis of each blade design alteration.

2.8.1. Design Space Analysis

Though the alterations to the blade design were initiated simultaneously with the alteration functions, each blade design alteration entailed a discrete change from the base case, allowing a sensitivity analysis to be undertaken with the One-at-a-Time (OAAT) method [33]. The impact of each blade design alteration on the suitability of the rotor for use in OSPR was then measured using the OSPR performance metrics. Initial assessments of the influence of each parameter informed the alteration range which was reasonable for each parameter - these decisions were based primarily upon acceptable levels of C_P and C_T, but also on the basic practicality of the blade design - e.g., designs with overlapping root chords were deemed impracticable.

A design space analysis method was developed to provide numerical-visual feedback of the impact on each performance metric. A design sub-space was required for each blade design parameter altered, in which the percentage change in the metrics was marked on a series of stacked y axes. The alteration range, as listed in Table 2, was set along a common x axis. Plotting the impact of one-at-a-time changes along x axes allowed the impact of individual parameter alterations to be studied, while at the same time intra-parameter trends and gradients over the alteration range were immediately obvious. Three design sub-spaces were created for the first stage blade design analyses - one for each parameter changed. These three spaces were stacked horizontally on a set of common y axes, giving the overall design space, allowing further comparisons to be drawn on an inter-parameter level. The inclusion of a conditional statement resulted in a variation in the marker type , indicating whether cavitation was predicted in each instance.

The design space of the first stage alterations is shown in Fig. 6.

2.8.2. Cavitation Analysis

The values of σ_{ir} and σ_r for each blade element were calculated and compared numerically for each blade design. As their definitions in Eqs. (13) and (15) indicate, these values were a function of λ; as λ increased, for each blade element, σ_r decreased towards the value of σ_{ir}. Plotting these two cavitation-related numbers against λ, for elements all along the blade, gave a more detailed visual tool to assess the occurrence, location(s) and extent of cavitation on the blade across the entire operating range. σ_{ir} was plotted for every element, giving a dense band of cavitation envelopes, beneath each strand of which cavitation would occur on the relevant blade section. The σ_r curves for the tip and root elements were plotted, along with those for the elements at increments of 10% of the blade length. For each blade iteration, comparison of these plots indicated whether the design alterations induced more or less cavitation along the blade.

2.8.3. Plots of α_r and dQ_r against r

The distribution of torque, Q, developed along the blade is heavily influenced by the twist and chord distributions. It was possible to undertake a deeper inspection of blade performance by considering the local

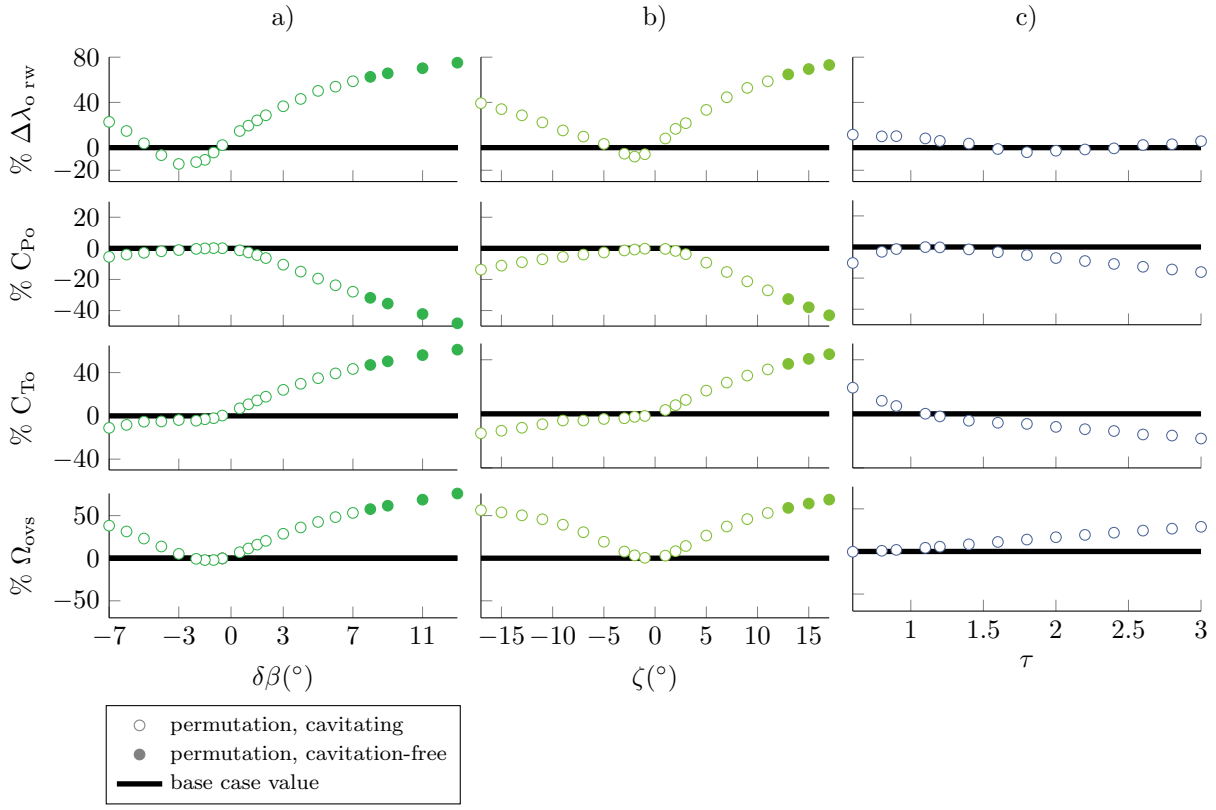

Figure 6: Design Space analysis, showing the results of the sensitivity analysis of OSPR performance metrics to first stage blade design parameter alterations to: a) the pitch setting, where +ve $\delta\beta$ changes indicate a root pitch which sets the root leading edge closer to the tidal flow vector; b) the twist distribution, where +ve ζ values indicate a blade with less twist along the span; and c) the chord distribution, where τ values greater than 1 indicate a blade with larger chord and cross-sectional area values.

α_r and the torque developed by each blade section, dQ_r. This was achieved using plots of the distribution of α_r and dQ_r across the blade, at the optimum and overspeed operating points. Analysis of these plots allowed important or influential sections of a blade design to be identified.

2.9. Stage Two Design Alterations

Analysis of the results from the Stage One design alterations showed that a Stage Two design process, using the same methodology, would be required to make alterations with which the requirement for further improvements in any performance metrics could be worked towards. Information from analyses of the first stage parameter alterations was fed forwards to this second stage, allowing for insightful design alterations.

3. Results and Discussion

3.1. Stage One

3.1.1. Design Space Results

The design space results from the first stage of blade design parameter alterations are presented in Fig. 6. For reference, Fig. 4 illustrates examples of the kind of design alterations made to produce these results. These plots showed that there were only seven blade permutations which eradicated cavitation, four resulting from alterations to β, and three from alterations to θ_r. Each of these blade designs had significantly reduced efficiency.

The sensitivity analysis showed that the primary metric, $\Delta\lambda_{\text{o rw}}$, was least sensitive to the applied c_r alterations. For the same degree of alteration, the sensitivity of $\Delta\lambda_{\text{o rw}}$ was greater to the alterations applied to β than to those applied to θ_r, having a greater rate of change in the former. As Fig. 2 shows, positive additions or alterations, respectively, to the twist or pitch reduced the angle between the tidal flow and the chord line at more blade stations, pointing the leading edge of the aerofoil section towards the incoming flow; in both cases this gave a positive impact on $\Delta\lambda_{\text{o rw}}$. The finding that blade designs with alterations of positive ζ and $\delta\beta$ values resulted in a more rapid feathering of the blades as U_∞ increased was therefore to be expected. However, it was possibleto achieve slightly greater impact on this performance metric by large alterations to θ_r than by the largest alterations applied to β. Alterations of more than 13° to β resulted in a blade with such poor efficiency that no power regulation was required at all; giving a limit to the possible positive alterations to β.

These two parameter alterations were also seen to have the greatest impact upon the second metric, Ω_{ovs}. Predicted cavitation inception was accordingly eradicated by alterations of $\delta\beta$ before alterations of ζ by the same degree. Reflecting on the resulting α_r for each blade section from these alterations, this is not surprising.The improvements in the first two metrics made by alterations to β and θ came at the great expense of reductions in C_{Po}. The impact of altering β was greatest, with the consequence that the first cavitation-free blade permutations - with $\beta = 8$ ° and $\zeta = 13$ ° - had a similar C_{Po}, changed by -31.8 ° and -32.6 ° respectively from the base case. As he $\alpha - r$ plots indicated that this decrease in C_{Po} occurred due to the resulting α for each blade station moving away from the optimum value, at which lift force per drag force is maximised.

A significant, but reduced impact was made in this metric by scaling alterations made to the chord length. This impact was due to the increase in the lifting surface associated with an increase in chord length, and, as the plots of α and dQ showed, an increase in the values of α occurring over the blade, each of which increased the torque produced.

The performance metric C_{To} was most sensitive to changes in β, its sensitivity having, again, a steeper gradient in response to $\delta\beta$ alterations than either ζ or scaled-c_r alterations. Alterations to β made in the positive sense reduced C_{To}, whereas those made in the negative sense had a detrimental effect on this metric. This was due to increases in α_r along the blade, resulting in an overall greater contribution to force in the axial direction (along the x axis). That the metric C_{To} was sensitive, though to a lesser degree, to the scaling alterations in c_r was, as for the impact on C_{Po}, due to the increase in the lifting surface producing greater lift and drag forces, resulting in a greater or lesser contribution to force in the axial direction for vales of τ smaller or greater than 1, respectively.

3.1.2. Cavitation Results

Fig. 7 c) shows the cavitation analysis plot for the full-scale base case design. The vertical decrease in σ_r in the region $0 \leq U_\infty \leq U_{\infty\text{max}}$ can be seen in this figure, occurring at $\lambda_o \approx 5$; no cavitation was predicted in this operation range. Cavitation was, however, predicted to begin occurring at the tip of the blade, at roughly $\lambda = 6.1$. The plot showed that cavitation incidence occurred at lower blade positions as λ increased. An interesting results from the plot is that after λ of 7.5, the tip of the blade was no longer the position with highest σ_{ir}, its value being exceeded by those of elements in the region of the root. However, because the σ_r values of the upper elements were very low, and those of the lower elements were comparatively high, cavitation continued to be more of an issue for the former than for the latter.

Cavitation was a consistent flow behaviour on most of the rotors in the first stage of design changes. As previously noted, seven blade designs were successful in mitigating cavitation inception: those with parameter changes of $\delta\beta \geq 8°$ and $\zeta \geq 13°$. The cavitation plot of the latter blade permutation is shown in Fig. 7 d). However, as indicated in the design space, these alterations also resulted in a significant drop in C_{Po} and increase in C_{To}, neither of which are useful rotor performance characteristics.

Through comparisons between this method and experiments it was found, in [23], that the use of XFoil to generate the C_{pres} data was a reliable method for preliminary design stages. It is important to note, though, that it was also found that this over-predicted cavitation on the upper surface of the aerofoil; this method is therefore known to give a slightly conservative analysis of cavitation inception.

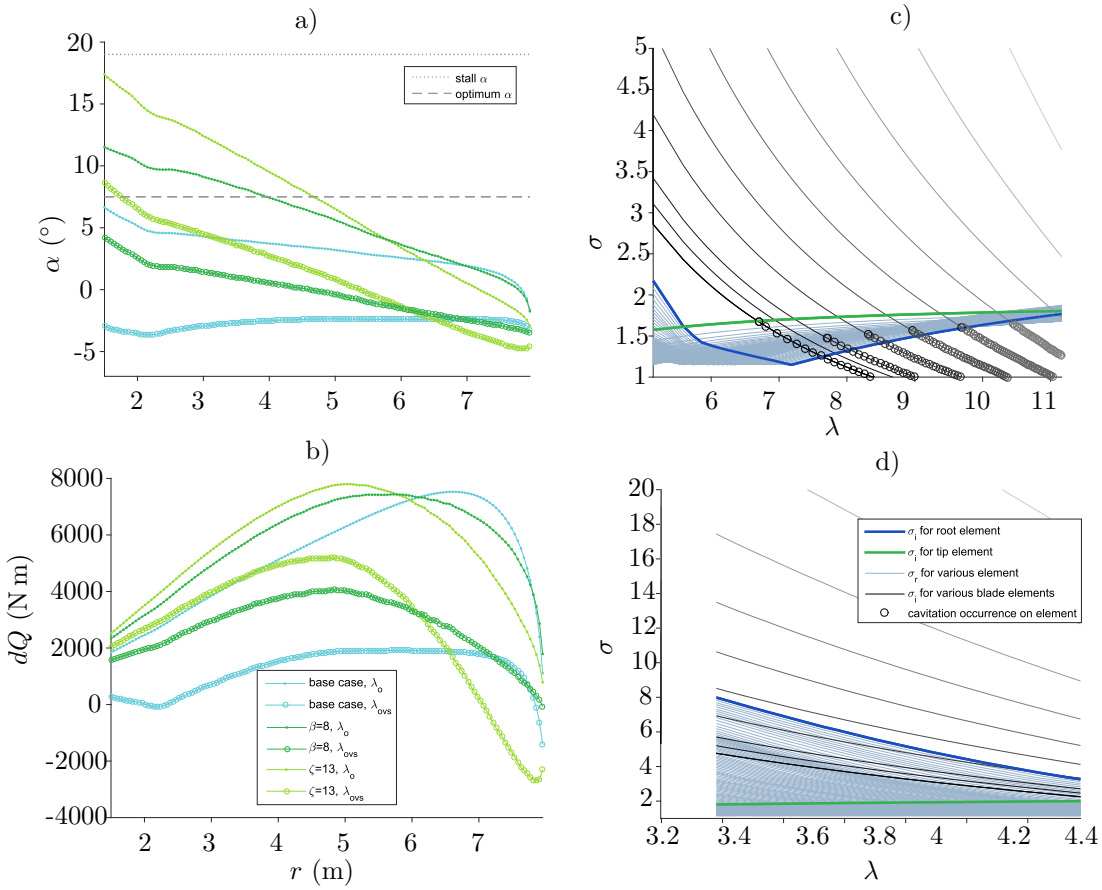

Figure 7: Plot of a) the local angle of attack and b) contribution to rotor torque on each blade section at the optimum and overspeed operating points for three blade designs showing the effect of the applied alterations; c) cavitation analysis for the base case blade; d) cavitation analysis for blade permutation $\zeta = 13$ °.

3.1.3. α_r and dQ_r Plot Results

Plots of local α and dQ for the base case blade, along with those of the non-cavitating blades with design alterations $\beta = 8°$ and $\zeta = 13°$, are shown in Fig. 7 a) and b). The plots of α_r in Fig. 7a) showed that, at λ_o, the mid sections of the altered blade designs were operating closer to the optimum α of 7.5. This gave rise to the increase in dQ seen for the mid-sections of these blades in Fig. 7b). The plots also showed that, due to the slower Ω at the optimum operating point, the root to mid sections of the altered blades were operating at much higher values of α, yet had not exceeded the stall angle, which (in the steady flow assumed) would ensure an equally stable working flow environment on these altered blade designs as on the base case blade.

Although the cavitation analysis for the blade of $\zeta = 13°$ design showed that no cavitation was predicted, the highly negative α_{tip} shown in Fig. 7a) was indicative of how close the blade tip was to cavitating - a result reflected, as shown in Fig. 7d), in the proximity of the relevant σ_r and σ_{ir} curves in this blade design's cavitation plot at λ_{ovs}.

3.2. Further stages of design alterations

Feedback from the Stage One design alteration process indicated that scaling up the size of all the aerofoils by the same factor had a similar scaling-type effect on the α, dQ over the blade. Considering the effect on the *distribution* of these parameters had by distribution alterations to the twist, the Stage Two alterations detailed in the relevant rows of Fig. 4 were made to the distribution of c_r. Proportionally linear increases were made to the chord length, increasing the chord to T, a proportion of the original chord tip length. To make use of the α_r values close to optimum on the blade mid-sections, the c_r distribution was altered with a parabolic added-chord function which peaked at values of ψ, a proportion of the original root chord length. It was possible in this way to have greater control over α across the blade, and thus to effect an altered distribution of dQ. This resulted in a similar impact in the metrics with - as integration of the c_r distribution terms showed - a similar overall increase in the blade area but, significantly, a reduced increase in the blade root chord length, leaving more room between blade roots. The design space result of this are presented in Fig. 8 a) and b).

In a series of Stage Three Alterations, blades with the chord distribution altered with T = 0.5 and $\psi = 1.4$ were coupled with alterations to θ_r of a range of ζ values. As Fig. 8 c) shows, predicted cavitation inception ceased when ζ reached 13 ° as before, but, as Fig. 9 indicates, C_{Po} was 42.4%, rather than the 32.0% of the Stage One blade. Such combined alterations as these were therefore found to be successful in continuing to allow cavitation-free regulation of power by overspeed while reducing the negative impact on C_{Po}.

Fig. 9 shows the power and thrust performance of key blade designs as progressive improvements were made with regards to suitability for OSPR. Comparison between the curves show that the indications of altered rotor performance given by the analysis tools had indeed been achieved. The operation of the rotor was been shifted towards lower λ values, with a more rapid drop-off in C_P on the RHS. And the drop in C_{Po} from the base case to the blade of $\zeta = 13°$ design was somewhat mitigated by alterations to the c_r. The value of C_{To} was also affected, in a similar manner to C_{Po}, suggesting that design alterations which improve C_{Po} will also increase C_{To} - an effect which may become a limiting criterion.

4. Conclusion

A blade design methodology for overspeed power regulated tidal turbine rotors has been developed, which considers the operation site and power regulation methodology within the design requirement-based boundary conditions. Blade design parameter alterations have been made and assessed using three visual-numerical analysis tools: a design space analysis based on overspeed performance metrics; a full-blade cavitation analysis over the entire operation range expressed with plots of converging cavitation and pressure curves; and plots of local angle of attack and torque distribution across the blades.

It has been shown that, between the applied parameter alterations, changes to twist distribution and pitch setting are most effective at reducing the rotor's maximum angular velocity within the operating range and thus mitigating the inception of cavitation and reducing the maximum terminal voltages with which the system must be built to cope. These alterations, however, come at the expense of a reduction in optimum

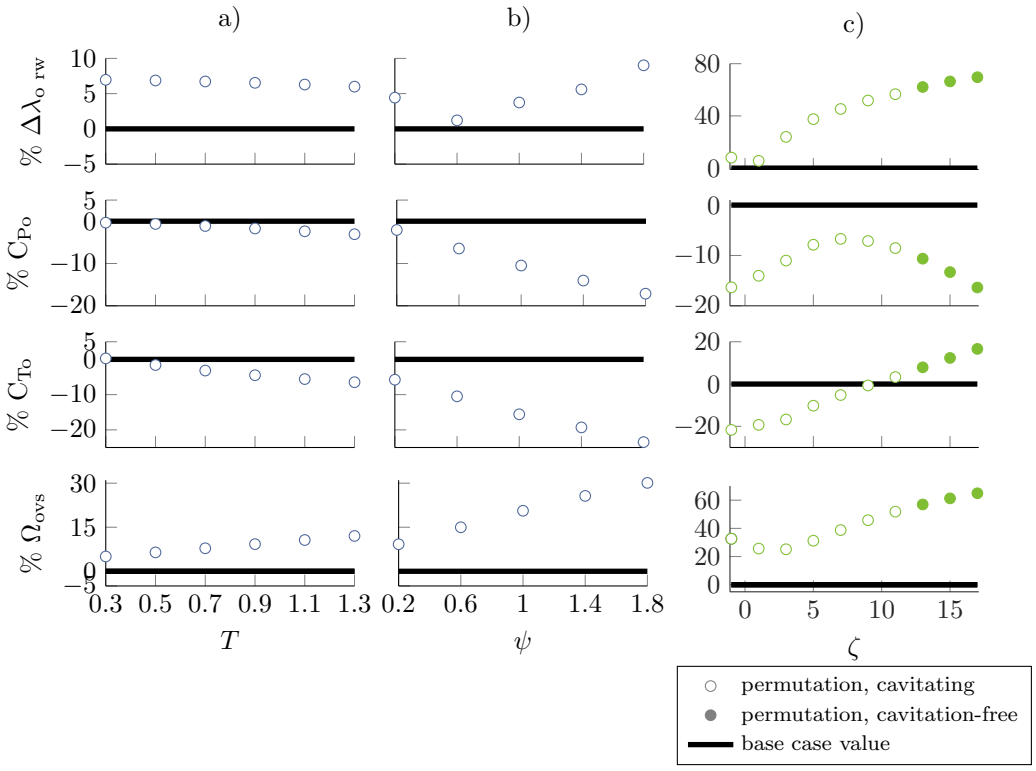

Figure 8: Design Space analyses of: a) and b) targeted alterations to c_r; c) combined alterations to c_r and θ_r.

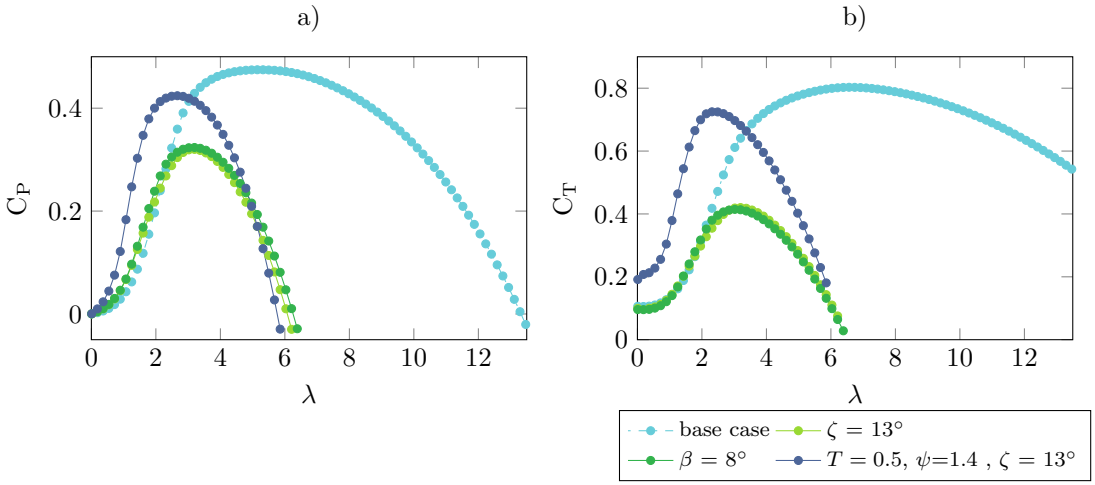

Figure 9: Characteristic performance curves of base case, stage-one alteration and coupled-alteration blade designs showing progressively more appropriate performance for application in OSPR tidal turbines

efficiency. While changes to the cross-sectional area of the blade via scaling and distributional alterations to the chord length have a lesser effect on the performance, these changes can be coupled with alterations to twist distribution to bring the optimum efficiency back towards acceptable levels without detrimental impact on the cavitation behaviour. Such coupled changes also affect the maximum coefficient of thrust and the effect this has on the turbine will need to be taken into account.

Cavitation analyses of the base case and altered blade designs have indicated that cavitation inception is an issue which should be considered, and which, depending on the aerofoil section and boundary conditions - site velocity profile and depth and turbine configuration - and may be a main driver for speed-limiting design alterations to blades for use in OPSR.

4.0.1. Insight Gained from Analysis Tools

Analysis of the first stage of design alterations showed that several of the discrete parameter alterations may bring about improvements in the OSPR performance metrics. The results from the tools used also suggested that localised parameter alterations coupled with initial discrete alterations may mitigate some of the detrimental effects from the initial alterations. For example, it was identified on inspection of $\alpha_r - r$ plots such as those in Fig. 7 that blade tips often had significantly lower α_r than the lower blade elements, resulting in the greater proximity, or cross-over of the σ_r and σ_{ir} curves for the tip elements, and leading to near or post-cavitation inception conditions. This finding suggested that localised θ_r alterations could be made to bring α_r to a less negative value at the blade tips. Use of the design methodology would enable the possible ramifications of such design changes to be analysed and compensated for with further insightful design alterations.

4.1. Future Work

The methodology will be applied to a blade design case study with specific design requirements setting the boundary conditions.

Verification exercises will be undertaken with tank tests of a prototype-scale blade, to confirm that altered blade designs perform as expected.

The methodology does not yet contain a structural integrity analysis. Further development of the methodology will take account of this, most likely with quasi-static structural integrity analyses. Nor has the effect of aerofoil shape been addressed; in future implementations of the methodology this will be investigated.

Inclusion of free-stream disturbance in the deployment environment would allow deeper analysis of the potential of this method of power regulation.

Acknowledgment

Grateful acknowledgements go to the wider Strathclyde and Dalhousie teams for valuable insight and help. This work has been funded by EPSRC through SuperGen Phase3, UKCMER. Further funding from UKSI, OERA and SDI has allowed the on-going collaboration between our two research groups. We would like to thank all of our funding bodies for their support.

References

[1] F. D. Bianchi, H. De Battista, R. J. Mantz, Wind turbine control systems. Principles, modelling and gain scheduling design., Vol. 26, Springer-Verlag London Limited, 2007.
URL http://dx.doi.org/10.1007/1-84628-493-7{_}2

[2] T. Ackermann, L. Söder, An overview of wind energy-status 2002, Renewable and Sustainable Energy Reviews 6 (1-2) (2002) 67–128. doi:10.1016/S1364-0321(02)00008-4.

[3] T. Burton, D. Sharpe, N. Jenkins, E. Bossanyi, Wind energy handbook, John Wiley & Sons Ltd., Chichester, 2001.
URL http://books.google.com/books?hl=en{&}lr={&}id=dip2LwCRCscC{&}oi=fnd{&}pg=PT14{&}dq=Wind+Energy+Hand+Book{&}ots=IbCMSqEsHb{&}sig={_}{_}fGWH60ILZ-30hDixeqjp7bVmU

[4] J. F. Manwell, J. G. McGowna, A. L. Rogers, Wind Energy Explained, John Wiley & Sons Ltd., Chichester, 2009.

[5] R. Pena, J. Clare, G. Asher, Doubly fed induction generator uising back-to-back PWM converters and its application to variable- speed wind-energy generation, Electrical Power Applications, IEE Proceedings 143 (3) (1996) 231–241.

[6] B. Whitby, C. E. Ugalde-Loo, Performance of pitch and stall regulated tidal stream turbines, IEEE Transactions on Sustainable Energy 5 (1) (2014) 64–72. doi:10.1109/TSTE.2013.2272653.
[7] E. Echavarria, B. Hahn, G. J. W. van Bussel, T. Tomiyama, Reliability of Wind Turbine Technology Through Time, Journal of Solar Energy Engineering 130 (3) (2008) 031005. doi:10.1115/1.2936235.
[8] Z. Zhou, W. Knapp, J. MacEnri, H. C. Sorensen, E. Friis Madsen, I. Masters, P. Igic, Permanent magnet generator control and electrical system configuration for Wave Dragon MW wave energy take-off system, 2008 IEEE International Symposium on Industrial Electronics (2008) 1580–1585doi:10.1109/ISIE.2008.4677255.
URL http://ieeexplore.ieee.org/lpdocs/epic03/wrapper.htm?arnumber=4677255
[9] A. Winter, Speed Regulated Operation for Tidal Turbines with Fixed Pitch Rotors, in: OCEANS 2011, Waikoloa, 2011, pp. 1–8.
[10] K. Gracie, R. E. Murray, C. M. Johnstone, D. A. Doman, M. J. Pegg, Fixed-Pitch Blades for Passive-Feather Power Regulation of Second-Tier Site Tidal Turbines, in: EWTEC, Aalborg, 2013.
[11] J. S. Carlton, Marine propellers and propulsion, second edi Edition, Elsevier Ltd., Oxford, 2007.
[12] C. Freeman, J. A. Teixeira, F. Trarieux, R. Ayre, Design of a gravity stabilised fixed pitch tidal turbine of 400kW, 8th European Wave and Tidal Energy Conference, Uppsala, Sweden, 2009 (2009) 376–383.
[13] A. Winter, T. Tryfonas, A constrained optimisation process for the design of tidal turbine blades with experimental validation (3).
[14] F. Biskup, M. Arnold, P. Daus, R. Arlitt, M. Hohberg, Effects of Rotor Blade Tip Modifications on a Tidal In-Stream Energy Converter – Voith HyTide ®, in: EWTEC, Aalborg, 2013.
[15] R. Starzmann, N. Hirsch, M. Baldus, S. Scholl, A stepwise approach towards the development and full-scale testing of a marine hydrokinetic turbine (2013) 1–6.
[16] K. Gracie, T. Nevalainen, C. Johnstone, R. Murray, D. Doman, M. Pegg, Impact analysis of blade shape on performance of tidal turbine for passive feather power regulation. Poster presentation, in: International Conference on Ocean Energy, Halifax, 2014.
[17] W. Batten, a.S. Bahaj, a.F. Molland, J. Chaplin, Hydrodynamics of marine current turbines, Renewable Energy 31 (2) (2006) 249–256. doi:10.1016/j.renene.2005.08.020.
URL http://linkinghub.elsevier.com/retrieve/pii/S0960148105002314
[18] M. J. Lawson, Y. Li, D. C. Sale, Development and verification of a computational fluid dynamics model of a horizontal-axis tidal current turbine, Proceedings of the ASME 2011 30th International Conference on Ocean, Offshore and Arctic Engineering (October).
[19] D. A. Doman, R. E. Murray, M. J. Pegg, K. Gracie, C. M. Johnstone, T. Nevalainen, Dynamic testing of a 1/20th scale tidal turbine, in: AWTEC, Tokyo, 2014.
[20] D. A. Doman, R. E. Murray, M. J. Pegg, K. Gracie, C. M. Johnstone, T. Nevalainen, Tow-tank testing of a 1/20th scale horizontal axis tidal turbine with uncertainty analysis, International Journal of Marine Energy 11 (2015) 105–119. doi:10.1016/j.ijome.2015.06.003.
URL http://dx.doi.org/10.1016/j.ijome.2015.06.003
[21] M. Drela, XFOIL: An analysis and design system for low Reynolds number airfoils (1989). doi:10.1007/978-3-642-84010-4{_}1.
URL http://link.springer.com/chapter/10.1007/978-3-642-84010-4{_}1
[22] D. V. Val, L. Chernin, Reliability-Based Design of Rotor Blades in Tidal Stream Turbines, in: European Wave and Tidal Energy Conference, Southampton, 2011.
[23] a. F. Molland, a. S. Bahaj, J. R. Chaplin, W. M. J. Batten, Measurements and predictions of forces, pressures and cavitation on 2-D sections suitable for marine current turbines, Proceedings of the Institution of Mechanical Engineers, Part M: Journal of Engineering for the Maritime Environment 218 (2) (2004) 127–138. doi:10.1243/1475090041651412.
URL http://pim.sagepub.com/lookup/doi/10.1243/1475090041651412
[24] H. C. Buckland, I. Masters, J. a. Orme, T. Baker, Cavitation inception and simulation in blade element momentum theory for modelling tidal stream turbines, Proceedings of the Institution of Mechanical Engineers, Part A: Journal of Power and Energy 227 (4) (2013) 479–485. doi:10.1177/0957650913477093.
URL http://pia.sagepub.com/lookup/doi/10.1177/0957650913477093
[25] R. Evans, R. McAdam, M. Royle, L. Mcewen, Optimum geometry for axial flow free stream tidal turbine blades, 10th European Wave and Tidal Energy Conference (EWTEC 2013), Aalborg, DK, 02. - 05. Sep 2013.
[26] J. L. V. Ingen, The eN method for transition prediction. Historical review of work at TU Delft, in: Fluid Dynamics Conference and Exhibit, no. June, Seattle, 2008, pp. 1–49.
[27] M. Drela, H. Youngren, XFOIL 6.9 User Primer (2001).
[28] D. M. Somers, The S814 and S815 Airfoils October 1991 — July 1992 The S814 and S815 Airfoils (December).
[29] W. Batten, a.S. Bahaj, a.F. Molland, J. Chaplin, The prediction of the hydrodynamic performance of marine current turbines, Renewable Energy 33 (5) (2008) 1085–1096. doi:10.1016/j.renene.2007.05.043.
URL http://linkinghub.elsevier.com/retrieve/pii/S0960148107002133
[30] R. F. Nicholls-Lee, S. R. Turnock, S. W. Boyd, Simulation based optimisation of marine current turbine blades, International Conference on Computer and IT Applications in the Maritime Industries (2008) 314–328.
URL http://eprints.soton.ac.uk/id/eprint/51108
[31] a.S. Bahaj, a.F. Molland, J. Chaplin, W. Batten, Power and thrust measurements of marine current turbines under various hydrodynamic flow conditions in a cavitation tunnel and a towing tank, Renewable Energy 32 (3) (2007) 407–426. doi:10.1016/j.renene.2006.01.012.
URL http://linkinghub.elsevier.com/retrieve/pii/S0960148106000516

[32] 26th ITTC Specialist Committee on Uncertainty Analysis, ITTC - Recommended Procedures 7.5-02-01-03. Fresh water and seawater properties, Tech. rep., International Towing Tank Conference (2011).
URL http://ittc.sname.org/CD2011/pdfProcedures2011/7.5-02-01-03.pdf

[33] D. M. Hamby, A review of techniques for parameter sensitivity analysis of environmental models., Environmental monitoring and assessment 32 (2) (1994) 135–54. doi:10.1007/BF00547132.
URL http://www.ncbi.nlm.nih.gov/pubmed/24214086